Preprint of an article submitted for consideration in Reviews of Accelerator Science and Technology Vol. 9 (2016)

SLAC-PUB-16810

Dielectric Laser Accelerators: Designs, Experiments, and Applications

K. P. Wootton

SLAC National Accelerator Laboratory
2575 Sand Hill Rd, Menlo Park, California 94025, USA
wootton@slac.stanford.edu

J. McNeur

Department of Physics, Friedrich-Alexander-Universität Erlangen-Nürnberg
Staudtstrasse 1, 91058 Erlangen, Germany
joshua.mcneur@fau.de

K. J. Leedle

Department of Electrical Engineering, Stanford University
450 Serra Mall, Stanford, California 94305, USA
kleedle@stanford.edu

Novel laser-powered accelerating structures at the miniaturized scale of an optical wavelength ($\sim$1 μm) open up a pathway to high repetition rate, attosecond scale electron bunches that can be accelerated with gradients exceeding 1 GeV/m. Although the theoretical and computational study of dielectric laser accelerators dates back many decades, recently the first experimental realizations of this novel class of accelerators have been demonstrated. We review recent developments in fabrication, testing and demonstration of these micron-scale devices. In particular, prospects for applications of this accelerator technology are evaluated.

Keywords: Dielectric laser accelerators, electron linear accelerators, free-electron lasers, lithography, attosecond science.

1. Introduction

Since the first conceptualization of a laser-powered electron linear accelerator (linac) [1], various laser electron linac schemes have been proposed and demonstrated. In this review, we summarize the crucial technological developments and underlying physical principles of recently demonstrated microstructure dielectric laser accelerators (DLAs). Building on prior reviews [2–7], in the present work we emphasize recent results and potential near-term and future technological opportunities for these miniaturized electron linear accelerators.

This article is organized into several main sections. The motivation of the DLA is first outlined through the historical context of relevant scientific and technological developments. We then present an overview of various proposed microstructure geometries. The operating principles of demonstrated microstructures and recent experimental results are summarized. Finally, we outline prospects for near-term applications of DLA accelerator components fabricated and integrated 'on-a-chip'.

2. Historical context

Criteria for the acceleration of charged particles by an electromagnetic field are given by the Lawson-Woodward theorem [8–11]. Succinctly, charged particles will not be accelerated by an electromagnetic wave if all of the following criteria are met [12]:

(i) The particle is in vacuum, far from any material surface;
(ii) The field is a far field (plane wave), integrated over an infinite interaction length;
(iii) The particle is relativistic;
(iv) No static electric or magnetic fields are present, yielding a particle trajectory which is approximately straight;
(v) The interaction is between the electromagnetic field and a single particle.

Thus, acceleration of charged particles requires that one or more of these conditions be broken. Several strategies can be adopted, in particular, the introduction of a near-field structure, with feature sizes governed by the drive wavelength, that modifies the

This material is based upon work supported by the U.S. Department of Energy, Office of Science, Office of Basic Energy Sciences, under Contract No. DE-AC02-76SF00515.

phase of incident wave fronts [13, 14]. This is the approach used in conventional radiofrequency linear accelerators, employing a conducting near-field structure [8]. A comprehensive summary of acceleration theorems and their relevance to various acceleration schemes can be found in Ref. [15].

One approach to accelerate charged particles using a laser is the abrupt termination of an incident field at a boundary [16–19]. Several experimental demonstrations have been made of electron acceleration by laser pulses at single-boundary structures, evading the Lawson-Woodward theorem [20–24]. Such structures may prove useful as a diagnostic of femtosecond (and shorter) electron-photon interactions [25–27], however they present practical difficulties in staging as a high-gradient laser-driven linear accelerator.

Several early proposals employing open structures were based on reflective (all-metallic) gratings, employing a wavelength-scaling of existing linear accelerator designs [15, 28, 29]. The acceleration mechanism employed in those demonstrations was the inverse Smith-Purcell effect [30].

The earliest proposal of a staged dielectric laser accelerator and focussing device was based on a periodic structure [31, 32]. It employed absorptive thin metal gratings deposited onto flat dielectric surfaces. This structure functioned through the use of an amplitude mask with a period matching the wavelength of the incident electric field. Conceptually similar radially-symmetric geometries were subsequently proposed [33, 34], though the assumed geometry of structures significantly larger than λ prevents their acceleration of relativistic particles [35]. Ultimately, it was not clear that metal deposited on dielectric surfaces was going to have the required laser damage threshold for high gradient accelerators.

Laser-driven structure-based accelerators were considered either to be composed of planar dielectrics [8, 36, 37], or metallic gratings as a wavelength-scaled miniature linac [14, 38, 39]. Evanescent fields near a single grating or dielectric slab could be used to accelerate sub-relativistic charged particles, however the accelerating modes of the inverse Smith-Purcell effect were synchronous only with sub-relativistic particle velocities [8]. What was required was local confinement of the evanescent fields using a dual-sided structure [8]. The enabling breakthrough was combining the grating design with dielectric materials. An early proposal suggested to modulate the phase of a laser field by a stepped grating using the refractive index of a dielectric [40], however that study significantly over-estimated the material damage threshold.

Initial work on DLAs was stunted by a misunderstanding of the damage mechanism: proposals were either pessimistic about the damage threshold of dielectrics ($200 - 400$ MeV/m [8, 35]) or overly optimistic [40]. The material damage mechanism of ultrafast laser pulses (ps and fs) is surface ablation, rather than being due to impurities in the bulk material (as with ns laser pulses). As a result, the material damage threshold (in terms of the maximum field gradient sustainable in the structure material) is significantly higher for ultrashort pulses [41–43]. With an understanding of the damage mechanism of the structure [44, 45], engineered DLAs have emerged.

Thus, the time is ripe for the development of accelerators powered by ultrafast laser technology. Recent technological developments in lasers have made infrared femtosecond lasers readily available [46]. When based on a fiber architecture, such lasers will be uniquely scalable for particle accelerator applications [47]. Lasers are also highly desirable as an accelerator power source owing to their high energy efficiency [48, 49], an important consideration in planned future accelerators [50, 51]. Due to the linear interaction of the accelerating fields in DLAs, their utilization is potentially both efficient and scalable.

Furthermore, microfabrication techniques driven by the semiconductor industry have advanced to the point of feasible fabrication of DLA microstructures [52–54]. The μm-scale wavelength results in feature sizes of order 400 nm: such structures are readily fabricated using conventional ultraviolet lithography. In addition, electron beam lithography is a convenient fabrication process for expedient prototyping of new structure geometries [55]. DLAs have emerged at the interface of these blossoming technological developments.

3. Microstructure geometries

In the case of the planar grating structure and even in more general terms, DLAs operate via laser-induced excitation of an electromagnetic field mode with a nonzero electric component parallel to the velocity of electrons traversing the mode. For long distance,

synchronous interaction to occur, the phase velocity of the excited mode must match the electron velocity. A wide variety of nanostructured dielectric geometries have been considered to efficiently excite such near-field modes.

3.1. *Bragg mirrors*

One such geometry consists of two planar Bragg mirrors separated by a vacuum channel through which electrons travel [56]. Each Bragg mirror is designed in such a way that the light reflecting off each interface within the mirror constructively interferes, leading to field confinement in the vacuum channel. A defect is introduced by changing the thickness of the dielectric layers adjacent to the channel. This allows for control of the phase velocity of the accelerating mode confined therein in order to satisfy the synchronicity condition. Light can be coupled into the cavity via dielectric coupling slots [57].

This planar Bragg geometry has been extensively simulated (yielding the fields shown in Fig. 1) and fabricated [58–60]. Due to the resonant nature of this design, accelerating gradients as much as ten times the incident field are possible [58].

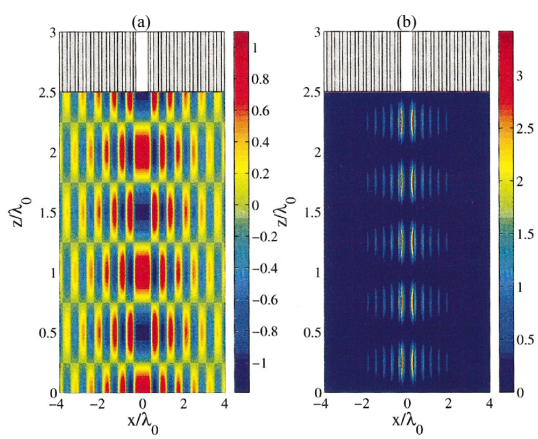

Fig. 1. Profile of fields within a planar Bragg mirror structure, with the distributed Bragg reflector profile illustrated at the top. The electron and laser beam propagate in z, with the vacuum channel centered at $x = 0$. (a) Longitudinal electric field, E_z normalized by the peak field. (b) Poynting vector, normalized by $|E_0|^2/\eta_0$, where η_0 is the intrinsic impedance. Reprinted figure with permission from [A. Mizrahi and L. Schächter, *Phys. Rev. E* **70**, 016505 (2004)]. © 2004 by the American Physical Society.

3.2. *Slab geometry*

The refraction of an inclined incident laser beam on a slab structure leads to a speed of light accelerating mode [8, 36, 61]. A structure employing such refraction at the interface of silicon-silicon carbide sample has been proposed [62]. Because silicon carbide is a polar semiconductor, its dielectric permittivity is negative for the mid-infrared wavelengths of CO_2 lasers. As a result, at the interface between a bulk silicon substrate and a silicon carbide thin film, evanescent waves are supported. Schemes in which laser light is coupled into this structure via gratings and prisms have additionally been proposed [63, 64]. These schemes have been tested for compatibility with CO_2 lasers.

3.3. *Photonic band-gap structures*

An alternative means of confining an accelerating field mode spatially is found through the use of photonic band gap (PBG) crystals, such as the hexagonal rod lattice shown in Fig. 2 [65]. A defect is introduced to the lattice in the form of a large hole in its center, in which a transverse magnetic (TM) accelerating mode along which electrons travel is excited [66–68]. In such a structure, the radius of the lattice holes, the lattice periodicity, the radius of the defect hole, and the permittivity of the material affect the band gap properties. These parameters are carefully controlled to ensure the TM mode confined in the defect has a phase velocity matching the velocity of accelerated electrons.

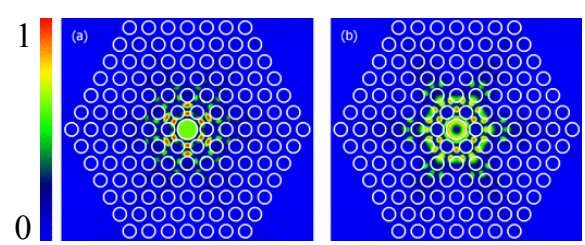

Fig. 2. Two dimensional photonic crystal lattice which supports a TM speed-of-light accelerating mode. Longitudinal (a) and radial (b) electric field magnitude of speed of light mode. Color scale indicates field relative magnitude. Adapted figure under CC-BY 3.0 license from [R. J. Noble, J. E. Spencer and B. T. Kuhlmey, *Phys. Rev. ST Accel. Beams* **14**, 121303 (2011)]. Published 2011 by the American Physical Society.

Various schemes for coupling laser light into modes propagating in the fiber have been studied us-

ing simulations [68, 69] and experiments [65, 70]. The accelerating mode can also be excited through an electron beam wake, which is another technique for direct characterization of speed-of-light fiber modes [71, 72].

Two dimensional PBG structures have been studied as DLAs [73]. These structures are infinite in one direction transverse to the electron velocity. A separate dual grating structure was also proposed employing ponderomotive focusing of electrons in addition to acceleration [74–76].

Three dimensional PBG structures – such as the so-called woodpile geometry shown in Fig. 3 – have also been proposed [77, 78]. The design is tailored in such a way that a TM mode is well-confined to the defect channel in the center of the photonic crystal. Indeed, a 300 MeV/m unloaded field gradient is expected along the electron axis of propagation. Further, the design has been fabricated via the sequential assembly of etched silicon layers to form a woodpile structure with a defect (electron beam channel) [79–81]. The structure has also been fabricated using 3D direct laser write [82]. Although this structure is amenable to the addition of ancillary devices such as couplers [81, 83, 84], coupling of light into the structure requires fabrication that has not yet been achieved due to restrictive error tolerances.

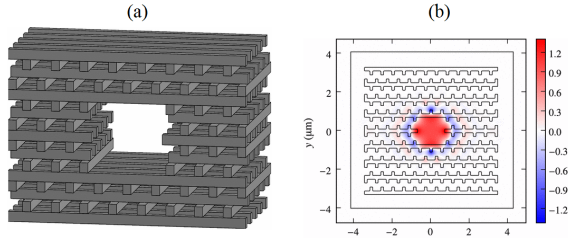

Fig. 3. Three-dimensional photonic crystal lattice. (a) Illustration of the woodpile structure, (b) Spatial profile of the confined accelerating field E_z, normalized to the electric field amplitude at the center of the vacuum defect. Adapted figure under CC-BY 3.0 license from [B. M. Cowan, *Phys. Rev. ST Accel. Beams* **11**, 011301 (2008)]. Published 2008 by the American Physical Society.

3.4. *Plasmonic structures*

An alternative to all-dielectric structures is the use of metal surfaces to create resonant structures [85]. A structured metal surface with antenna slots at periodic spacings offers a means to locally enhance the electric field 10-15 times the incident laser field [86, 87].

Recently, plasmonic metasurfaces have been proposed as an engineered laser accelerator surface [88–90]. The proposed structure is composed of a staggered array of slots and antennas in a thin metallic surface in order to enhance the accelerating gradient. A critical parameter to be measured will be the metasurface damage threshold at the operating laser wavelength.

3.5. *Grating structures*

Grating DLA structures of various geometries are transversely driven by pulse-front tilted or multiple drive laser beams to excite a grating mode. Several grating geometries have been proposed [91], with basic variations illustrated in Fig. 4.

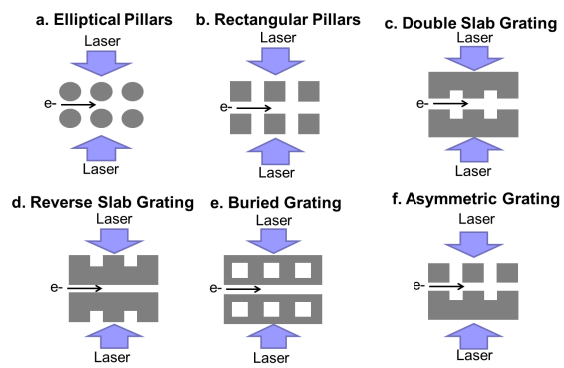

Fig. 4. Basic designs of two-dimensional gratings suitable for building dielectric laser accelerators. (a) elliptical dual pillar grating [92] (b) rectangular dual pillar grating [93, 94] (c) dual slab grating [95, 96] (d) reverse slab grating [97] (e) buried grating structure [98, 99] (f) asymmetric grating (any combination of the above, including elliptical and rectangular features).

Elliptical and rectangular dual pillar designs (Fig. 4a, b) are fabricated with 2D lithography from a monolithic substrate [92, 97]. They have high refractive contrast and can produce a variety of photonic crystal modes, and elliptical dual pillar gratings have been experimentally demonstrated [92]. Elliptical dual pillar gratings have relaxed fabrication requirements compared to rectangular pillars, although monolithic 1D rectangular dual pillar gratings can be fabricated using a wafer heterostructure and selective etches. Alternatively, a rectangular dual grating could be fabricated by overlapping two orthogonal

1D gratings to obtain very sharp corners in a 2D monolithic grating design.

The dual slab grating (Fig. 4c) uses 1D gratings and has low aspect ratio etches [95, 96, 100]. It also has a solid substrate attached to the gratings for efficient heat removal and optical alignment, but requires wafer bonding. Both the dual slab grating and reverse slab grating (Fig. 4d, [97]) could be fabricated monolithically with 2D top-down lithography. The 2D reverse slab grating and the buried grating (Fig. 4e, [98, 99]) both have the advantage of having solid and smooth vacuum channel sidewalls for the electrons, which could provide advantages for reduced electron scattering, better charge control and integration with on-chip waveguides. Finally, any of the previously described gratings can be mixed and matched to make an asymmetric grating (e.g. Fig. 4f), which could have advantages for specific applications. For example, a rectangular pillar grating combined with a slab grating provides a monolithic, 1D dual grating structure.

Resonance effects in the thickness of single gratings have also been explored in simulation [101]. In that study, the substrate thickness was $\sim\lambda$, which could be particularly relevant for optimization of pillar structures. Further work remains on exploring the effect of so-called guided mode resonances in the case of finite laser pulse lengths, transverse laser spot sizes, and finite geometries.

3.6. *Deflecting and focusing structures*

Deflecting structures are integral components of particle accelerators [102–104]. Indeed, undulators for free-electron lasers have been designed using deflecting microstructures illuminated by alternating pulse-front tilted laser beams to define each pole [102, 105]. Alternatively, the undulator could utilize lithographically-defined undulator poles, requiring only a single pulse-front tilted laser beam as the driver [106].

In addition, periodic focusing of the electron beam must be provided. Several focusing arrangements using laser-driven grating structures have been proposed. In such arrangements, focusing is provided by symmetric pumping of the structure using two lasers [107, 108]. Additionally, a single grating focusing structure based on a parabolic grating tooth geometry has recently been proposed and demonstrated [109].

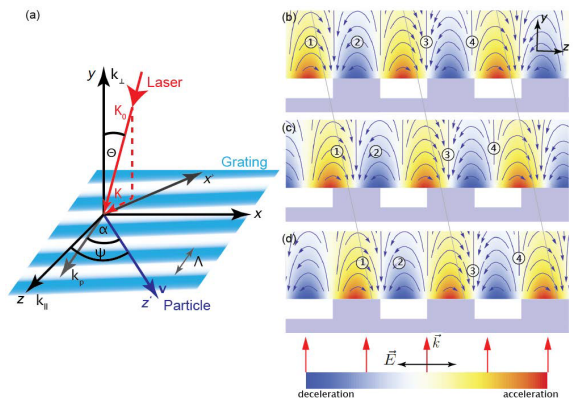

Fig. 5. (a) The geometrical setup of a laser incident upon the single grating. (b)-(d) Three snapshots of four charged particles traversing a single grating, illuminated by a laser. The simulated field pattern is shown. Depending on the injection phase of the positron in the excited accelerating wave, the positron can be either accelerated, decelerated or deflected. Adapted figure with permission from [J. Breuer, J. McNeur and P. Hommelhoff, *J. Phys. B: At. Mol. Opt. Phys.* **47**, 234004 (2014)]. © IOP Publishing. Reproduced with permission. All rights reserved.

4. Fundamentals of grating and pillar structures

Since 2013, three particular DLA geometries have been used to demonstrate dielectric laser acceleration experimentally. These are the single grating [110, 111], dual-grating [95, 96, 112, 113], and dual pillar structures [92, 94, 114]. We describe each of these in the following sections.

4.1. *Single grating*

Due to ease of fabrication and experimental testing, the single grating dielectric geometry shown in Fig. 5 and its variants (discussed below) have recently been tested. When illuminated by a perpendicular laser pulse (see Fig. 5), a near field diffracted field pattern is excited above the surface of the grating. This field pattern can be decomposed into a Fourier sum of traveling waves in the z direction in Fig. 5. In the geometry where $\alpha = \psi = \theta = 0$, the field profile of each of these traveling waves can be analytically described as [115]:

$$E_z = \frac{icB_0}{\kappa\gamma} e^{i(k_{nz}z + k_{ny}y - \omega t + \phi)}, \quad (1)$$

$$E_y = \frac{-cB_0}{\beta} e^{i(k_{nz}z + k_{ny}y - \omega t + \phi)}, \quad (2)$$

$$B_x = B_0 e^{i(k_{nz}z + k_{ny}y - \omega t + \phi)}. \quad (3)$$

Here, c is the speed of light, B_0 is the amplitude of the transverse magnetic field, κ is the ratio of the grating periodicity to the incident wavelength, $\gamma = \left(1-\kappa^2\right)^{-1/2}$, ω is the circular frequency of the incident laser, $k_{nz} = n\omega/\kappa c$, $k_{ny} = k_{nz}/\gamma$ and n is the index of the mode. In order for the fields to synchronously accelerate electrons traveling in the z direction above the grating (and injected at the appropriate phase), the phase velocity of the $n = 1$ traveling wave, $\omega/k_{1z} = \kappa c$ equals the injection velocity of electrons, βc. A limiting factor of the single grating DLA arises from the transverse decay of the accelerating fields in the y-direction, dictated by $k_y = k_z/\gamma = \omega/\gamma\kappa c$. Thus, the accelerating field has a decay length of $\beta\lambda\gamma/2\pi$.

4.2. *Dual grating*

The evanescent fields of a single grating structure are not suitable for acceleration of relativistic particles ($\gamma \gg 1$) [8]. This is because the position of the evanescent mode with speed of light velocity occurs at a distance of ∞ from the grating surface, where the amplitude of the field is zero [110, 116, 117]. However, the fields between two dielectric surfaces (or gratings) are suitable because the superposition of evanescent waves traveling in opposite directions (along the y-axis – either due to reflection off of the second surface or a second incident source) results in a hyperbolic cosine transverse profile, rather than an exponential decay [110, 116]. The first proposal of such a geometry was as a miniature linac [8]. A design employing dielectric dual gratings was subsequently proposed [40]. Recently, dual grating structures designed for fs lasers were developed, as illustrated in Fig. 6.

The dual grating structure operates as a phase-reset structure [40]. In the simplest geometry, the accelerator structure is a dielectric slab with a binary grating of structure period $\Lambda = \beta\lambda$. The 'phase-reset' arises from the phase difference between refraction through a dielectric pillar of refractive index $n > 1$, compared to a vacuum region with $n = 1$. The grating structure is designed to support evanescent grating modes propagating upwards and downwards through the structure. In the case of a pure TM mode accelerating structure ($\alpha = \psi = 0$), within a structure period these diffraction modes U_n, V_n and W_n in the z, y, and x directions, respectively can be de-

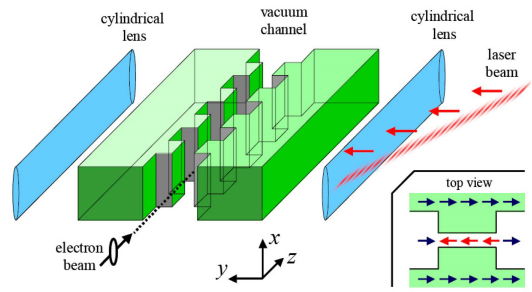

Fig. 6. Dual grating dielectric laser accelerator microstructure, illuminated from one side by a pulse-front tilted laser beam. Adapted under CC-BY 3.0 license from [T. Plettner, P. P. Lu and R. L. Byer, *Phys. Rev. ST Accel. Beams* **9**, 111301 (2006)]. Published 2006 by the American Physical Society.

noted by [103]:

$$U_n(y) = u_{n,+}e^{+\Gamma_n y} + u_{n,-}e^{-\Gamma_n y}, \quad (4)$$

$$V_n(y) = v_{n,+}e^{+\Gamma_n y} + v_{n,-}e^{-\Gamma_n y}, \quad (5)$$

$$W_n(y) = w_{n,+}e^{+\Gamma_n y} + w_{n,-}e^{-\Gamma_n y}, \quad (6)$$

where the modes u, v, w are the amplitudes of the upwards and downwards (reflected and transmitted) propagating diffraction modes in the z, y, and x directions, respectively. The coefficient of the nth grating diffraction order Γ_n is given by:

$$\Gamma_n = \sqrt{\left(nk_p - k\sin\theta\right)^2 - k^2} \quad (7)$$

where θ is the angle of incidence of the laser to the structure (typically $\theta = 0$), $k = 2\pi/\lambda$, and $k_p = 2\pi/\Lambda$, where Λ is the structure period. Summing over all modes, the fields can be described by the Fourier series [103]:

$$E_z(y,z,t) = \sum_{n=-\infty}^{+\infty} U_n(y)e^{iz(nk_p - k\sin\theta)}e^{ikct-i\phi}, \quad (8)$$

$$E_y(y,z,t) = \sum_{n=-\infty}^{+\infty} V_n(y)e^{iz(nk_p - k\sin\theta)}e^{ikct-i\phi}, \quad (9)$$

$$B_x(y,z,t) = \sum_{n=-\infty}^{+\infty} W_n(y)e^{iz(nk_p - k\sin\theta)}e^{ikct-i\phi}, \quad (10)$$

where ϕ corresponds to the phase between the electron and incident laser. Assuming that the electron travels in the $\vec{z}$ direction, then the average force on

a particle is [103]:

$$\langle F_z \rangle = q\mathbb{R}\left\{ \frac{1}{s\left(T\right)} \int_0^{s(T)} \sum_{n=-\infty}^{+\infty} U_n(y) e^{iks/\beta - i\phi} \times e^{is(nk_p - k\sin\theta)} \mathrm{d}s \right\}, \quad (11)$$

$$\langle F_y \rangle = q\mathbb{R}\left\{ \frac{1}{s\left(T\right)} \int_0^{s(T)} \sum_{n=-\infty}^{+\infty} V_n(y) e^{iks/\beta - i\phi} \times e^{is(nk_p - k\sin\theta)} \mathrm{d}s \right\}, \quad (12)$$

$$\langle F_x \rangle = 0, \quad (13)$$

where $s(T) = \beta c T$ is the distance traveled by a particle in time T. In practice, relativistic TM mode structures are designed such that $\langle F_z \rangle \gg \langle F_y \rangle$ for relativistic electrons. The appearance of a small but nonzero F_y occurs because the structure is pumped asymmetrically from one side only. With two laser beams (incident simultaneously from above and below), there is cancellation in this transverse force arising from symmetry in the upwards and downwards propagating laser modes [103, 116]. Experimental demonstrations of relativistic beams in DLAs have not observed measurable deflection from an asymmetrically-pumped accelerating structure [96, 118]. However, significant transverse deflecting forces can be imposed on the particle if the grating is rotated such that $\alpha \neq 0$ [102, 103].

Structures are designed to operate with peak electric fields provided by ultrafast femtosecond laser pulses. Pulses of order 100 fs are routinely available, but limit the interaction length to ∼30 μm (of order 50 DLA periods). The interaction region can be extended by employing pulse-front tilt [91, 95]. Pulse-front tilt of an incident laser pulse is illustrated in Fig. 6, occurring when an optical pulse encounters a dispersive element (diffractive or refractive).

Many numerical optimization studies of the dual grating structure have been undertaken, for different laser wavelengths, dielectric materials and electron beam energies [107, 112, 113, 119–121]. These optimizations principally use finite-difference time-domain (FDTD) or finite-difference frequency-domain (FDFD) electromagnetic simulations. Such optimizations are usefully employed to identify appropriate microfabrication techniques.

From the perspective of electron beam quality, the impedance that micro-fabricated corrugated dielectric accelerator structures present to the beam is significant [122]. Related accelerator structures have been proposed, whereby the phase gratings are recessed with a smooth, continuous vacuum channel surface for the electron beam [62–64, 98, 123]. Additionally, the proposed structure could be fabricated by etching the structure in one dimension into the wafer. This eliminates the need to bond wafers, which can introduce phase misalignment between the top and bottom gratings reducing the accelerating gradient [99].

4.3. *Dual pillars*

Two rows of dielectric rods represent the simplest implementation of a dual grating dielectric laser accelerator with the minimum material used. Additionally, due to the high refractive index contrast of a dual pillar structure and the lack of any substrate material affecting the optical mode, a wide variety of optical modes can be engineered with this simple geometry. Particle accelerators based on dual pillar gratings can be traced back to Palmer [39] for radio frequency applications with metallic rods. Rows of dielectric rods can be used to create high reflectivity mirrors for transverse-magnetically polarized light, creating a strongly modulated optical near field for electron acceleration. Moreover, dual pillar gratings can create a variety of coupled accelerator modes with hyperbolic cosine or hyperbolic sine mode profiles in the same way as the dual slab grating.

The constituent block of a dual pillar structure is a single row of pillars that will produce evanescent inverse Smith-Purcell grating modes on either side [92]. The thickness of the pillars controls the optical delay across each pillar and hence interference between the incident and exciting optical fields interacting with the pillar grating. With sufficient refractive index contrast (e.g. silicon:vacuum has 3.5:1 refractive index contrast), a pillar can produce a $\pi/2$ phase modulation between the vacuum gaps between pillars and the pillars themselves, canceling out the transmitted optical field and creating a high reflectivity grating with a strongly modulated evanescent periodic mode. Using partially transmissive gratings and/or dual sided illumination allows excitation of a hyperbolic coupled mode between the two rows of pillars with ultrashort laser pulses.

5. Recent experimental results

Several recent experiments have demonstrated electron acceleration using DLAs of various geometries. Briefly, these experimental results are outlined.

5.1. *Single grating demonstrations*

Many variations of these dielectric single gratings have been tested with sub-relativistic electron beams. An experimental setup used to test such structures with a 20-30 keV electron beam is detailed elsewhere [110]. At the time of those first experiments, the apparatus consisted of a scanning electron microscope serving as a DC electron source, a Ti:Sapphire long-cavity oscillator (generating pulses with a pulse length of 110 fs, a central wavelength of 787 nm, a pulse energy of 150 nJ, and a repetition rate of 2.7 MHz), a 4-axis actuator stage to align the electron beam and laser pulses to the DLA, and a detection system consisting of a high-pass energy filter (a retarding field spectrometer) and a microchannel plate detector.

In practice, the voltage of the retarding field spectrometer is set higher than the injected electron energy divided by the electron charge. For instance, if the injected energy is 25 keV, the spectrometer voltage is set to 26 kV so that only electrons who have gained an energy of 1 keV or more as they pass the DLA traverse the energy filter and reach the MCP detector.

This setup was used for the first proof of principle dielectric laser acceleration of sub-relativistic electrons [111]. In that experiment, a fused silica single grating with a periodicity of 750 nm was illuminated by the aforementioned Ti:Sapphire laser. This periodicity, limited by fabrication capabilities, meant that the third spatial harmonic was used for accelerating electrons with an injection energy of approximately 28 keV. The dependence of the resulting acceleration signal on the spectrometer voltage, laser polarization, distance of the electron beam from the surface of the grating, and the injection energy of the electrons is shown in Fig. 7.

A significant step enabling new fabrication techniques for DLAs was the first demonstration of acceleration and deflection using a DLA fabricated from silicon [124], in which a 96.3 keV electron beam was accelerated with a gradient of 218 MeV/m and deflected with a gradient of 160 MeV/m. The structure used in that experiment was a single grating with 490 nm pitch designed to phase match with the fundamental spatial harmonic of a 130 fs, 5 nJ Ti:Sapphire oscillator at 907 nm wavelength. This corresponded with longitudinal energy gains of up to 1.2 keV for acceleration and transverse energy gains of 0.9 keV for deflection. Acceleration and deflection were measured simultaneously using an imaging spectrometer. Silicon is a desirable DLA material principally because of the ubiquity of fabrication techniques that can be employed to integrate the accelerator with other optical components such as on-chip wave guides. Moreover, its relatively high index of refraction at optical and near-infrared wavelengths leads to efficient coupling of incident laser light into the desired accelerating mode. Since that experiment, several other DLA structures have been fabricated in silicon, some of which are described below.

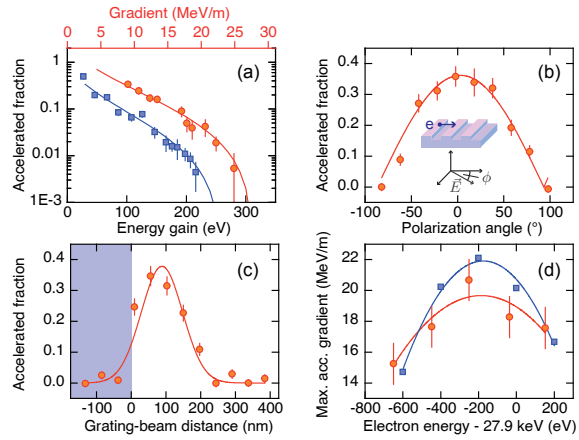

Fig. 7. The detected electron count rate for the experimental setup described in Sec. 5.1 as a function of the spectrometer voltage (a), the polarization of the incident laser (b), the distance of the electron beam centroid from the surface of the grating (c) and the injection energy of the electrons (d). Reprinted figure with permission from [J. Breuer and P. Hommelhoff, *Phys. Rev. Lett.* **111**, 134803 (2013)]. © 2013 by the American Physical Society.

The electron beam experimental setup in Ref. [111] was recently upgraded via the use of Si single gratings (with a period of 620 nm) with a Tm-fiber laser operating at a central wavelength of 2 μm, a pulse energy of 1 μJ, a pulse length of 500 fs, and a repetition rate of 1 MHz. The periodicity of the grating and the incident wavelength ensured that 28 keV electrons would be synchronously accelerated by the first harmonic above the grating.

Moreover, the transverse decay of the accelerating mode scales with the incident wavelength, so that the size of the region of strong accelerating fields is more than twice as large when compared with the previous proof of principle experiment, lending motivation towards working with 2 μm lasers in DLA experiments. Electrons with energy gains approaching 1.5 keV were detected, a five-fold increase when compared to the proof of principle experiment [111].

The smallest feature size that can be fabricated using conventional lithography is of the order of 300 nm, which constrains the range of electron beam energies that can be accelerated by the first spatial harmonic of the structures. However, lower electron energies (velocities) can be accelerated at DLAs by using harmonics of the fundamental spatial mode. Experiments at single gratings with the third, fourth and fifth harmonics have demonstrated acceleration of electrons with kinetic energy as low as 9.6 keV with an acceleration gradient of 7.5 MeV/m [125, 126].

For a grating geometry with a fixed periodicity, the velocity of accelerated sub-relativistic electrons will eventually no longer match the phase velocity of the accelerating traveling wave. Thus, electrons slip in phase with respect to the traveling wave. Electrons injected at accelerating phases encounter decelerating phases after a length determined by the electron energy, laser wavelength, and field gradient. This must be compensated for by either frequency chirping the incident laser pulse or modifying the acceleration structure design, where the phase velocity of the accelerating mode has to match the particle velocity at all longitudinal coordinates. A design, based on lithography-based structural chirping, that aims to achieve this is shown in Fig. 8.

In the chirped structural design [109], the distance between grating teeth depends on the longitudinal coordinate z as $\lambda_p = \lambda_{p0} + az$, where $\lambda_{p0} = 620$ nm is the starting grating period and a the chirp parameter. In Fig. 9 the accelerated electron current as a function of $eU_s - E_{k0}$ is shown for different values of a but the same laser parameters, with e the electron charge and U_s the DC voltage applied to the spectrometer. The maximum energy gain is now limited by the incident field amplitude of $E_{\max} = 1.3$ GV/m and the interaction distance which in turn is given by the laser spot radius $w = 29 \pm 3$ μm. Without any structural chirp

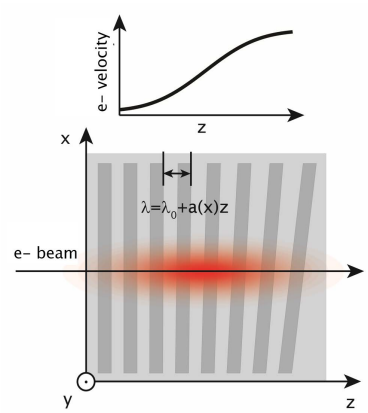

Fig. 8. The chirped structural design that overcomes the so-called dephasing of accelerated electrons. The grating period increases as electrons travel in the positive z-direction. Further, the slope of increasing grating period (a) is a function of the position over which the electrons pass the structure in the x-direction, allowing for this parameter to be tuned in situ [109].

($a = 0$), dephasing limits the maximum achievable energy gain to $\Delta E_k = 0.80$ keV, in agreement with theory [115]. For $a = 6.5 \times 10^{-4}$, the maximum energy gain is more than tripled to $\Delta E_k = 2.6$ keV, corresponding to an acceleration gradient of 69 MeV/m.

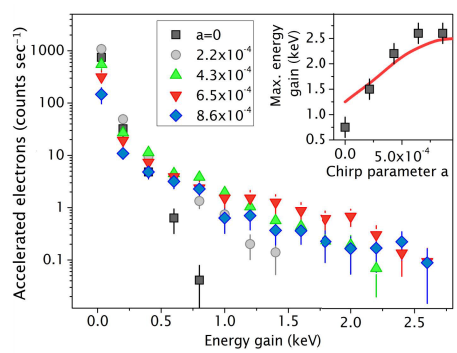

Fig. 9. The accelerated count rate as a function of the minimum electron energy gain for various chirp parameters a, The dephasing limit is overcome for chirp parameters $a > 0$ [109].

5.2. *Dual grating demonstrations*

Dual grating experiments have been conducted using relativistic electron beam energies in the range of 8–60 MeV. The incident electron beams were accelerated by conventional radiofrequency linear accelerators upstream of the DLA [127–131]. Several facilities for dual grating DLA experiments with non-

relativistic [132–135] and relativistic electron beams have subsequently been proposed [136–140].

The first demonstration of dielectric laser acceleration at relativistic energy was performed using a dual-grating structure [96, 141, 142]. The structures were fabricated from fused silica [53, 54, 143], and driven by a $\lambda = 800$ nm Ti:Sapphire laser with 1 ps pulse duration. In that experiment, a maximum electron accelerating gradient of 350 MeV/m was observed.

A factor of DLAs that was not accounted for at the time of early theoretical research is that the peak breakdown field of the material is strongly dependent upon the pulse duration [41]. In effect, for a given incident fluence, reducing the incident laser pulse duration increases the electric field of the accelerator. This was experimentally demonstrated recently through acceleration of relativistic electrons using fs-scale laser pulses at a dual grating structure [118]. Employing laser pulses of 90 fs duration, a peak accelerating gradient of 690 ± 100 MeV/m was observed. Results are illustrated in Fig. 10.

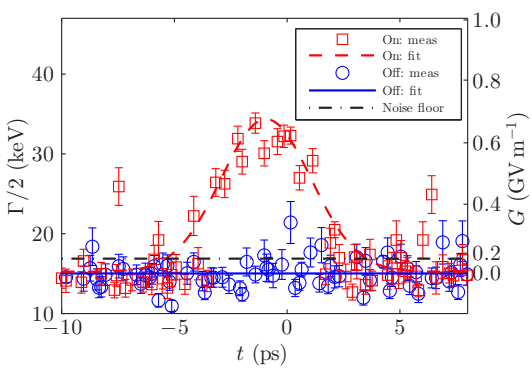

Fig. 10. Scanning the time of arrival of the accelerating fs laser pulse relative to the time of arrival of the electron bunch. With the laser on, the half-width at half maximum of the energy electron beam energy distribution ($\Gamma/2$) was increased. A peak accelerating gradient of 690 ± 100 MeV/m was observed. Reprinted figure with permission from [K. P. Wootton, *et al.*, *Opt. Lett.* **41**, 2696 (2016)]. © 2016 by the Optical Society of America.

In experiments accelerating electron beams using DLAs, the energy spread of the incident electron beam is modulated. This arises because the incident electron bunch of ∼100 fs duration is much longer than the DLA structure with period ∼3 fs. An appropriately bright source with microbunching elements (Sec. 6.2), is necessary to match the restrictive longitudinal phase-acceptance of DLA buckets. At relativistic energy, a phase-stable train of electron microbunches has been achieved using an inverse free-electron laser, resulting in net acceleration after interaction with an optical-scale accelerator [23, 24]. Sources designed for shortest electron bunches have been demonstrated using velocity bunching [144], which may also be combined with nanotip photocathode sources with demonstrated low transverse emittance [145–147].

5.3. *Resonant structures*

A Bragg mirror structure was developed as a slab-symmetric, resonant DLA. The bandpass of the resonant structure was demonstrated from optical transmission through the structure [58]. Electron beam tests were performed at the E-163 experimental end-station at SLAC with a 60 MeV beam and 100 fs Ti:Sapphire laser pulses [52, 58, 59, 148].

In experiments searching for acceleration with the structure, broadening of the transmitted energy spread was observed corresponding to an accelerating gradient of 28 MeV/m [149]. Further advances in the precision of the fabricated structures may be necessary to efficiently couple into the speed-of-light resonant accelerating modes.

5.4. *Dual pillar demonstrations*

The first monolithic dual grating DLA device demonstrated was a dual pillar structure made from a single piece of silicon [92]. Monolithic fabrication on a single wafer allows precise lithographic alignment of multiple structures and has strong advantages for future integrated accelerator devices. An example of a fabricated dual pillar structure is illustrated in Fig. 11.

Silicon dual pillar grating structures were demonstrated at sub-relativistic electron energies of 86.5 keV and 96.3 keV with a few nanojoule Ti:Sapphire oscillator drive laser [92]. By tailoring the pillar dimensions, both an inverse Smith-Purcell accelerating mode (exponential transverse profile of mode, analogous to a single grating) and an evanescent coupled mode (cosh transverse profile, analogous to a dual grating) were demonstrated. The inverse Smith-Purcell mode structure used a highly reflective pillar grating and a single drive laser, which only produced measurable excitation of one row of pillars. This structure produced maximum accelerat-

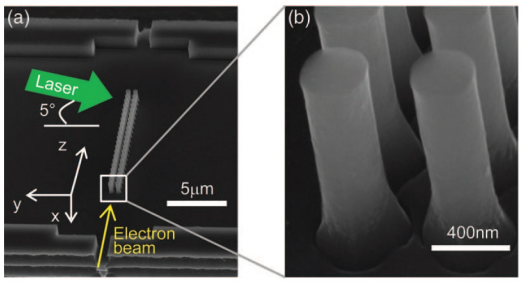

Fig. 11. Dual pillar structures fabricated in silicon for acceleration of sub-relativistic electron beams. Reprinted figure with permission from [K. J. Leedle, *et al.*, *Opt. Lett.* **40**, 4344 (2015)]. © 2015 by the Optical Society of America.

ing gradients of 370±40 MeV/m and 255±25 MeV/m deflecting gradients for longitudinal energy gains of 2.05 ± 0.02 keV and transverse energy gains of 1.43 ± 0.1 keV, respectively. The experimental maximum acceleration and deflection observed approached 35% and 24% of the incident laser field strength, respectively.

The evanescent coupled mode dual pillar structure used a partially reflective pillar grating to allow a single drive laser to excite the evanescent fields on both sides of the accelerator channel to form a cosh accelerating mode in the channel. This coupled cosh mode produced uniform accelerating gradients of up to 196 ± 20 MeV/m with little beam deflection for electrons in the center of the coupled mode [92]. This was the first demonstration of a coupled mode with low deflection at sub-relativistic electron energies. Many of the other sub-relativistic experiments described are limited in laser-electron interaction length by the transverse deflection of the laser fields. Future experiments with optimized structures and two drive lasers could enable higher acceleration gradients with a more robust low deflection hyperbolic cosh mode over extended accelerator lengths.

5.5. *Two stage acceleration demonstrations*

In order to verify the viability of phase-controlled staged acceleration, the authors in Ref. [109] employed an optical variation to the setup described in Sec. 5.1. An interferometer-like setup is introduced that splits the incoming laser pulse into two pulses, which are then focused to two separate spatial regions on the single grating structure (see Fig. 12). Electrons encounter two laser pulses separated in time by 200 fs.

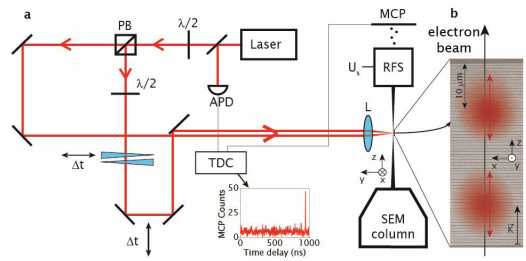

Fig. 12. Optical setup to create two distinct interaction regions for a single grating silicon DLA [125].

By varying the relative arrival time of the two pulses with a delay line with 200 attosecond precision, the experiment shifts between two regimes: one in which electrons that are accelerated in the first pulse are decelerated in the second pulse and one in which electrons are accelerated in both pulses, enhancing the total acceleration signal. The oscillation between these regimes, evidence of phase-controlled staging, is shown in Fig. 13. This has been used to imprint sub-fs interactions on an electron beam [150]. Moreover, this staging demonstrates the linear scaling of the energy gain with the interaction distance and with the number of stages.

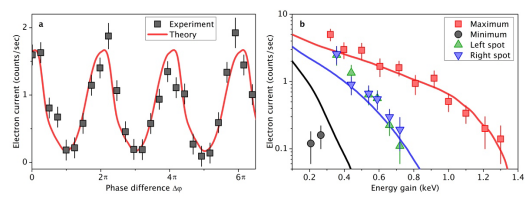

Fig. 13. The accelerated signal as a function of the relative phase of two laser pulses illuminating two distinct interaction regions. The signal oscillates between suppression and enhancement of acceleration. Moreover, the energy gain is roughly doubled in the enhanced regime (red) compared to interaction with each individual region (blue, green). [109]

5.6. *Focusing structure*

Silicon gratings have also been used to demonstrate focusing of a sub-relativistic electron beam, employing a design shown in Fig. 14 [109]. In a single grating structure, a deflecting mode can be excited by tilting the grating with an angle α with respect to the electron beam, as proposed in Ref. [102]. As the deflection angle φ of the electron depends linearly

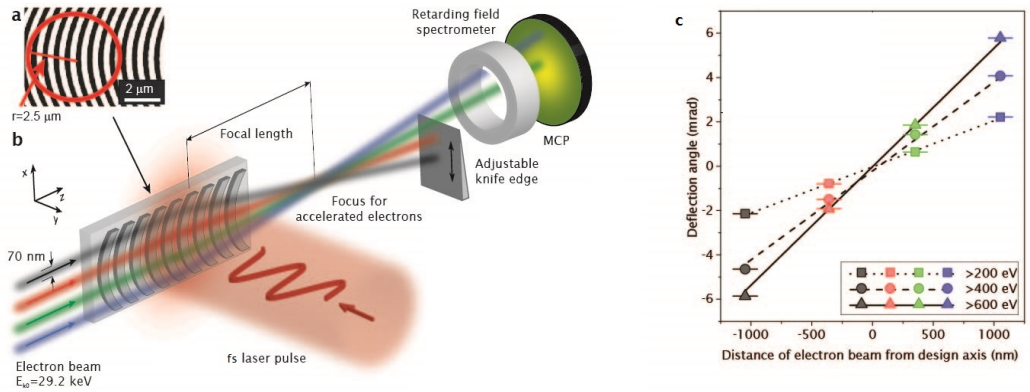

Fig. 14. A focusing DLA structure. (a) The radius of curvature of the grating teeth is illustrated. (b) The focal length of the structure was measured by translating the electron beam and a knife edge. (c) Different accelerated electron energies are focused with different focusing gradients, corresponding to the deflecting force at the appropriate optical phase [109].

on the grating tilt angle α, focusing can be achieved by a DLA microstructure with grating teeth with a parabolic transverse profile (so that the tilt angle of the grating tooth depends on the distance from the center of the design axis as $\alpha = \sigma x$, where σ is a constant and x is the distance from the design axis).

The focusing structure was demonstrated by translating an electron beam spatially in x across the structure, and observing the deflected position of the electron beam downstream. Hence the deflected angle φ could be measured, as illustrated in Fig. 14. The deflected angle φ was observed to be proportional to the offset x. That is, linear focusing was observed with $\varphi = bx$, with focal length $f = 1/b$. Transverse focusing and longitudinal acceleration are optical phase dependent in this DLA structure, and because electrons arrive randomly in the laser optical phase, the focusing strength and acceleration differ for electrons depending upon their optical phase. Effective focal lengths of the structure were determined for electrons with minimum energy gains of 200, 400, and 600 eV as 500 ± 20, 260 ± 10 and 190 ± 10 μm respectively for a structure with profile given by $\sigma = 0.39$ μm^{-1}.

6. Potential applications

A schematic illustrating the basic components of a DLA-based accelerator (Fig. 15) consists of multiple stages of acceleration and focusing elements illuminated by a single laser source. Moreover, the laser source could trigger a photocathode (e.g. a tungsten or lanthanum hexaboride nanotip) that would then serve as an electron source for the multi stage DLA. A future accelerator based on this architecture could enable many different applications [151]. Many interrelated questions remain, including the achievable pulse length and bunch charge from a laser-triggered nanotip, the handshake energy between the cathode and the first dielectric acceleration stage, and beam current stability of such a nanotip source [126]. However, a simple scaling argument can provide an estimate of the beam parameters for different applications.

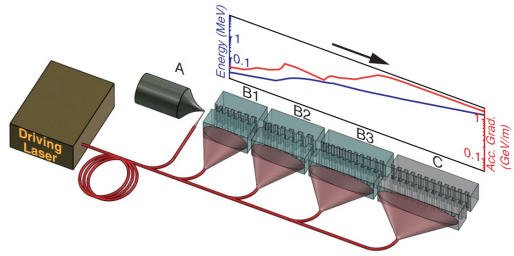

Fig. 15. Schematic illustration of an accelerator based on a nanotip emitter and successive DLA stages. Reprinted figure with permission from [J. Breuer and P. Hommelhoff, *Phys. Rev. Lett.* **111**, 134803 (2013)]. © 2013 by the American Physical Society.

For a 30 keV electron beam, such a device can support 80 electrons per accelerating bucket [115], where we assume a 2 μm drive wavelength, a 400 as bunch length and an emittance limited beam in which the perveance is treated as a perturbation. For a laser with a pulse length of 600 fs and a flat-top temporal profile, 7200 electrons per laser pulse can be supported. Further, for high repetition rate lasers (>1 MHz like in commercially available solid state

lasers), >10 nA of average current can be supported in a multi stage DLA. Further, the supported charge per bunch scales favorably with higher electron energy. Indeed, an optimal charge of >1 fC per bucket and >10 fC per bunch train is feasible for relativistic ($\beta \sim 1$) electrons [48, 49].

6.1. *Medical therapy*

Even modest nA current in a mm-scale MeV electron source would be of great benefit for medical patient treatment. While protons can be used to irradiate tissue deep inside the body, medical electron beams are limited to treatment of superficial cancers and diseases (within 6 cm of the patients surface) due to the energy deposition along the path from the surface to the tumor [152]. These beams operate at electron energies of 6-20 MeV. The generation of such an electron beam presently requires radio-frequency accelerators with a typical acceleration length of 1 m, and meter long beam delivery systems. The acceleration length is determined by the acceleration gradient, which is about 10-20 MeV/m, while the delivery system must enable localization and positioning of the electron beam to the tumor.

With a DLA and expected gradients exceeding 1 GeV/m the generation of MeV electron beams over an acceleration length in the millimeter to centimeter range should well be possible. With a compact source with micron scale beams the beam delivery complexities can be removed, and a significant improvement in the irradiation localization can be achieved. While a new form of tumor treatment might yield the largest benefit to society, other forms of medical applications may also be realized by this technology. Examples include endplate etching neurons, improving neuronal vesicle release and nerve function, as well as localized electron irradiation cleaning of sensitive devices (e.g. endoscopes with interior electronics).

With an active acceleration length on the millimeter to centimeter scale one may envision a multi-MeV electron beam generation device of the size of a tip of a pen, as illustrated schematically in Fig. 16. This would enable wholly new forms of electron beam treatments for clinicians, where, for example, the electron beam generation device is brought inside the body of a patient [153]. Because of the potentially close proximity of the electron source device to

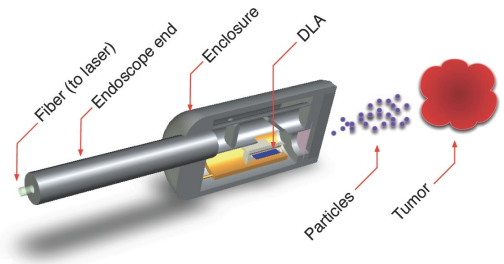

Fig. 16. A hypothetical schematic for the incorporation of a monolithic multi-stage DLA on an endoscope for the purpose of tumor irradiation. Reprinted figure with permission from [R. J. England, *et al.*, *Rev. Mod. Phys.* **86**, 1337 (2014)]. © 2014 by the American Physical Society.

the cancerous tissue, electron energies in the range of 1-5 MeV seem very promising, as the electrons are absorbed in the range of a few millimetres to about one centimeter [154]. Because of the small exposed volume, an electron current in the range of nA is sufficient to deliver a single massive dose over an exposure time on the order of 1 s, ideal for handheld or robotic surgery, with easily-removed heat loads in the Watt regime. This could be transformative for intraoperative electron radiation therapy (IOERT), a highly successful electron beam based precision cancer treatment employed for decades already [155–158]). So far, the space requirements of conventional accelerators have prevented full exploitation of the therapeutic potentials of IOERT in the clinic.

6.2. *Sub-optical cycle interaction*

In addition to the generation of relativistic electrons, DLAs have the capability of imprinting sub-optical cycle energy modulation onto free electrons. Hence, DLAs could be used to create sub-optical cycle electron bunches. The sub-cycle velocity modulation induced by the interaction of sub-relativistic electrons and laser-induced accelerating fields leads to ballistic microbunching if the electron beam drifts following the acceleration interaction. The simulated electron beam phase space for a one optical cycle long subset of the bunch is shown in Fig. 17 at different times after interaction with the silicon single grating described above [150]. At maximum compression, the bunch full-width half-maximum drops below 200 attoseconds for a 30 keV starting electron energy.

This velocity bunching approach places stringent requirements on the interaction strength and electron energy in order to form a single microbunch for

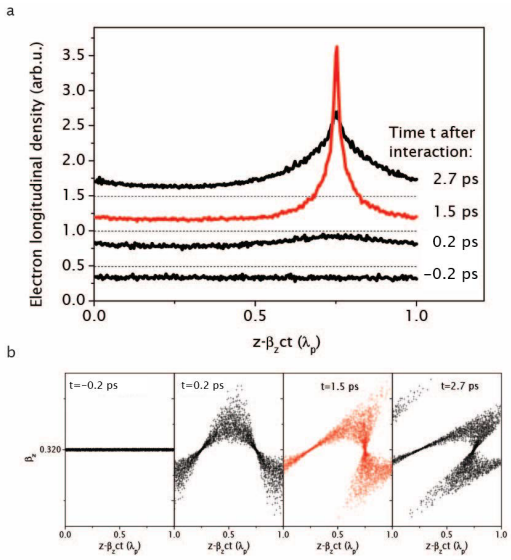

Fig. 17. Simulation of longitudinal velocity bunching of a sub-relativistic electron beam downstream of interaction with a DLA. (a) Longitudinal electron density at various times t after interaction with a DLA. It can be seen that optimal bunching occurs approximately 1.5 ps downstream of the interaction, with a FWHM less than 200 as. For clarity, the zero baseline (dotted line) is offset vertically by 0.5 arb. units between successive times. (b) Electron beam longitudinal phase space distributions corresponding to (a).

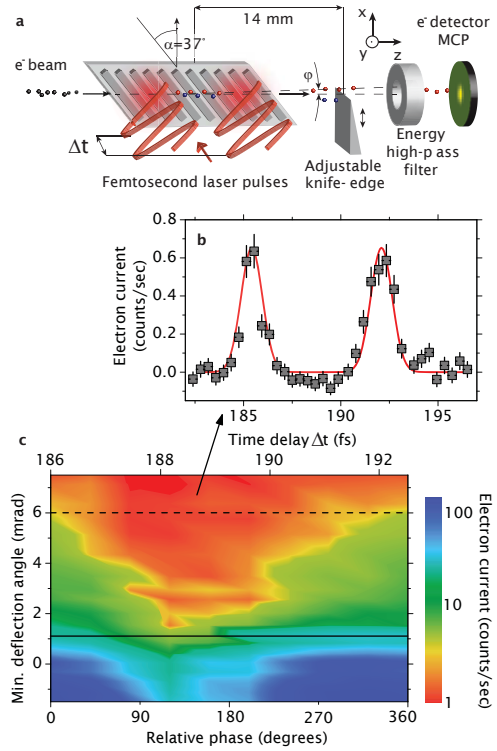

Fig. 18. The experimental design and results of a two-stage deflection experiment. Two sequential regions of a tilted single grating DLA are illuminated by laser pulses with a controllable relative phase delay. By monitoring the accelerated signal that is also deflected past an adjustable knife edge as a function of the relative phase delay of the pulses illuminating the two regions, feature sizes on the order of 1 fs are detected in the energy modulated electron beam. [150].

attosecond electron diffraction or other experiments. However, filtering the electron energy spectrum after interaction at two stages of deflecting structures enables the use of longer laser pulses to select out a single short temporal window. Consider the conceptual illustration in Fig. 18.

For this deflecting structure, electrons injected on crest are not only accelerated in z but deflected in x. Moreover, the deflecting force imparted onto the electrons depends on their injection phase. By illuminating two regions of the deflecting structure and varying the relative arrival time of the two 2 μm laser pulses illuminating the regions, the demonstrated timing resolution of such a diagnostic is revealed to be 1.3 fs. Employing ultrashort incident laser pulses (e.g. a 20 fs laser pulse length with a central wavelength of 2 μm) and "gratings" consisting of only one grating tooth, a sub-cycle energy modulation can be imprinted on a passing electron beam. By then using a high pass energy filter such as the high-pass spectrometer in Fig. 18, this sub-cycle (attosecond scale) feature could be isolated from the rest of the electron beam in an sub-optical cycle pump-probe experiment [150].

To realize a practical attosecond DLA streak camera, the evanescent decay of field strength at the single grating design must be overcome. With a single grating, the deflection angle of electrons is not only correlated with their arrival time at the interaction region but also with their arrival position with respect to the surface of the grating. Towards this end, a double grating design with a grating tooth tilt angle (shown in Fig. 19) is promising [102].

6.3. *Attosecond photon generation*

Extreme ultraviolet (EUV) sources are one option for lithographic fabrication of increasingly miniaturized microprocessor components [159, 160]. Over many decades, conventional accelerator light sources have matured to provide routine access to electromagnetic radiation from infrared through to hard X-rays

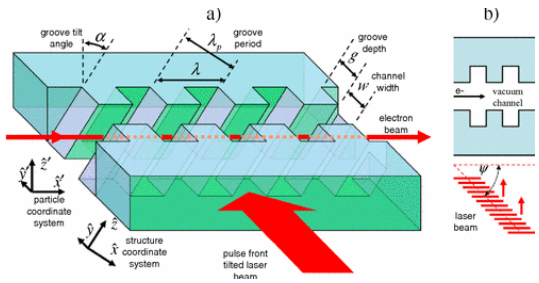

Fig. 19. A deflecting structure, driven by a pulse-front tilted laser beam synchronous with the relativistic electron velocity. Reprinted figure under CC-BY 3.0 license from [T. Plettner and R. L. Byer, *Phys. Rev. ST Accel. Beams* **11**, 030704 (2008)]. Published 2008 by the American Physical Society.

[161, 162]. The development of light sources targeted to EUV wavelengths presents a unique opportunity for future accelerator-based light sources [163–165]. A coherent light source was an early proposed application of microstructure accelerators [166]. Other ideas have been developed taking advantage of the unique attosecond bunch format produced by DLAs [167, 168].

The critical hardware component is the deflecting structure [102, 104, 105, 116]. With an electron traveling at a transverse angle to the accelerating direction of a DLA, a non-zero deflection force results [91] as presented in Sec. 6.2. An undulator composed of dielectric deflecting structures is desirable because the structures accommodate undulator periods $\sim 10 - 100$ μm, with deflecting fields exceeding 1.3 GeV/m, equivalent to a magnetic field of $\sim$4 T [102]. Such a structure can be optimized for deflection transverse to the direction of electron propagation rather than longitudinal acceleration [169, 170]. An undulator can be formed by staging several such structures sequentially, as illustrated in Fig. 20.

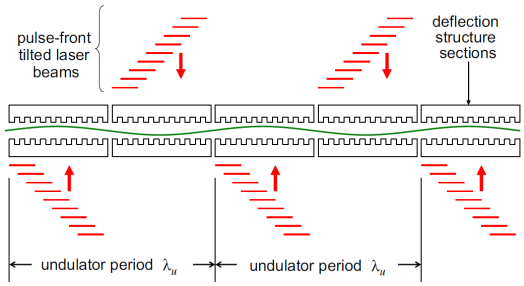

Fig. 20. An undulator composed of successive stages of laser-driven deflecting structures. Reprinted from [T. Plettner and R. L. Byer, *Nucl. Instrum. Methods Phys. Res., Sect. A* **593**, 63 (2008)], with permission from Elsevier. © 2008 by Elsevier.

Technological advances in lithography allow several simplifications to be made. Lithographic control of the microstructure phase means that single-sided illumination of the undulator poles could be employed instead of alternating at each pole [106].

6.4. *Beam position monitor*

To optimize accelerators with multiple stages and components, particle beam diagnostics are required. In particular, diagnostics of the transverse beam position and distribution are necessary for reliable operation. Given the transverse profile of electron beam channels in DLAs is on the order of $\sim$1 μm, beam diagnostics with fundamental resolution on the scale of nanometers are required.

A candidate scheme for a nanometer resolution transverse beam position monitor involves the inverse acceleration process. Compared to acceleration of electrons by pumping a DLA structure with laser fields, the inverse process occurs when an electron beam passes through the structure and radiates energy. The evanescent wakefields generated by the electron beam couple to the DLA structure, resulting in the emission of real photons as an electron passes through. This has been developed as a passive structure beam position monitor [108, 171–173], and as a beam-driven photon source [174]. The dual grating structure used is illustrated in Fig. 21.

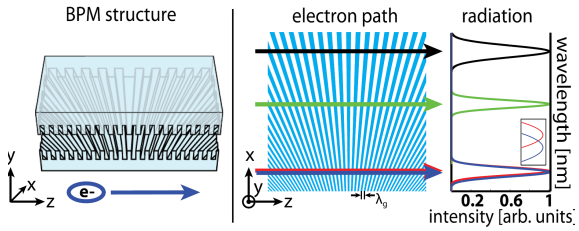

Fig. 21. Passive beam position monitor structure, based on dual grating DLAs with a period that varies in the transverse coordinate x. The beam position is determined from the wavelength of light emitted when electrons pass through the channel. Reprinted figure with permission from [K. Soong, *et al.*, *Opt. Lett.* **39**, 4747 (2014)]. © 2014 by the Optical Society of America.

Electrons within the vacuum channel of the dual grating DLA emit radiation perpendicular to the surface of the grating with a central wavelength matching the periodicity of the grating. The dual grating geometry ensures that the periodicity of the grating

depends on the transverse position of the beam in x. Thus, by monitoring the central wavelength and bandwidth of the emitted radiation, the centroid position and transverse spot size of the electron beam can be deduced. Using the 60 MeV, 20 μm wide electron beam from the Next Linear Collider Test Accelerator at SLAC, a spatial resolution of 10 μm was achieved [173]. With smaller electron beams, a spatial resolution of 0.7 nm is expected, which would be useful for the control of beams through successive stages of DLAs.

In addition, recently an active BPM structure has been demonstrated [175]. By pumping the structure with laser photons, cross-correlation of the arrival of the laser pulse and electron bunch at the structure was observed with a spatial resolution of ∼450 nm and temporal resolution of ∼480 fs. The experiment was conducted with a sub-relativistic electron beam, but the technique can be extended to relativistic energies through the use of a double-sided structure.

6.5. *TeV-scale linear collider*

We note that DLAs may be a viable technology candidate for a future 10 TeV electron-positron collider, as is argued in greater detail in Refs. [6, 151]. To reach such center-of-mass energies with microwave technology, a main linac over 100 km in length would be necessary, however a DLA linac of length of 10 km operating at GeV/m acceleration gradient could achieve the same energy. The required luminosity of such a collider (10^{36} cm^{-2} s^{-1} [6]) favors the DLA bunch format of low bunch charge operated at high repetition rates to avoid beamstrahlung energy spread at the interaction point, which scales with the bunch charge [151]. Lastly, we note that the existence of high repetition rate solid state lasers could lead to electrical wall-plug efficiency exceeding 10%, which is very favorable for proposed collider schemes [48, 49].

7. Summary

Dielectric laser accelerators compose a subfield of novel laser-based accelerators that, due to decades of innovative design development and laser and nanofabrication progress, has recently blossomed with experimental demonstrations of advanced beam diagnostics and manipulation as well as accelerating gradients approaching 1 GeV/m. With further advances, applications related to photon generation, radiative oncology and ultrafast metrology may soon be realized. We here summarize the history of the field, the many designs conceived within, and their recent experimental results.

Acknowledgments

The authors are grateful to Prof. Robert L. Byer (Stanford University), Dr. R. Joel England (SLAC National Accelerator Laboratory) and Prof. Peter Hommelhoff (Friedrich-Alexander-Universität Erlangen-Nürnberg) for comments that greatly improved the manuscript.

This work was supported by the U.S. Department of Energy under Contract DE-AC02-76SF00515, the U.S. Air Force Office of Scientific Research under grant FA9550-14-1-0190, the European Research Council under grant 616823 NearFieldAtto, and by the Gordon and Betty Moore Foundation under grant GBMF4744 (Accelerator on a Chip).

References

[1] K. Shimoda, *Appl. Opt.* **1**, 33 (1962).
[2] J. D. Lawson, in *Generation of High Fields for Particle Acceleration to Very-high Energies*, Tech. Rep. CERN-1985-007, CERN (Geneva, Switzerland, 1985). pp. 3–12.
[3] J. Arnesson and F. K. Kneubühl, *Infrared Phys.* **25**, 121 (1985).
[4] G. Travish and R. B. Yoder, *Proc. SPIE* **8079**, 80790K (2011).
[5] G. Travish, *AIP Conf. Proc.* **1507**, 85 (2012).
[6] R. J. England, *et al.*, *Rev. Mod. Phys.* **86**, 1337 (2014).
[7] R. J. England, *IEEE J. Sel. Top. Quantum Electron.* **22**, 4401007 (2016).
[8] J. D. Lawson, *Laser Accelerators?*, Tech. Rep. RL-75-043, Rutherford Laboratory (Chilton, Oxon, UK, 1975).
[9] J. D. Lawson, *IEEE Trans. Nucl. Sci.* **26**, 4217 (1979).
[10] J. D. Lawson, *Part. Accel.* **10**, 73 (1980).
[11] P. M. Woodward and J. D. Lawson, *J. Inst. Electr. Eng. - Part III: Radio Commun. Eng.* **95**, 363 (1948).
[12] R. B. Palmer, An introduction to acceleration mechanisms, in *Frontiers of Particle Beams*, eds. M. Month and S. Turner, Lecture Notes in Physics, Vol. 296 (Springer Berlin Heidelberg, 1988) pp. 607–635.
[13] R. B. Palmer, *Part. Accel.* **11**, 81 (1980).
[14] R. B. Palmer, *IEEE Trans. Nucl. Sci.* **28**, 3370 (1981).

[15] R. B. Palmer, *AIP Conf. Proc.* **335**, 90 (1995).

[16] E. Esarey, P. Sprangle and J. Krall, *Phys. Rev. E* **52**, 5443 (1995).

[17] T. Plettner, *Analysis of Laser-Driven Particle Acceleration from Planar Infinite Conductive Boundaries*, Tech. Rep. SLAC-PUB-11637, Stanford Linear Accelerator Center (Menlo Park, CA, USA, 2006).

[18] T. Plettner, *Analysis of Laser-Driven Particle Acceleration from Planar Transparent Boundaries*, Tech. Rep. SLAC-PUB-11800, Stanford Linear Accelerator Center (Menlo Park, CA, USA, 2006).

[19] T. Plettner, *Field-Analysis of Vacuum Free-Space Laser Acceleration from Rough-Surface and Absorbing Thin Boundaries*, Tech. Rep. SLAC-PUB-13188, Stanford Linear Accelerator Center (Menlo Park, CA, USA, 2008).

[20] Y. C. Huang, *et al.*, *Nucl. Instrum. Methods Phys. Res., Sect. A* **407**, 316 (1998).

[21] T. Plettner, *et al.*, *Phys. Rev. ST Accel. Beams* **8**, 121301 (2005).

[22] T. Plettner, *et al.*, *Phys. Rev. Lett.* **95**, 134801 (2005).

[23] C. M. S. Sears, *et al.*, *Phys. Rev. ST Accel. Beams* **11**, 101301 (2008).

[24] C. M. S. Sears, *et al.*, *Phys. Rev. ST Accel. Beams* **11**, 061301 (2008).

[25] F. O. Kirchner, *et al.*, *Nat. Photonics* **8**, 52 (2014).

[26] A. Gliserin, M. Walbran and P. Baum, *Rev. Sci. Instrum.* **87**, 033302 (2016).

[27] C. Kealhofer, *et al.*, *Science* **352**, 429 (2016).

[28] Y. Takeda and I. Matsui, *Nucl. Instrum. Methods* **62**, 306 (1968).

[29] K. Mizuno, S. Ono and O. Shimoe, *Nature* **253**, 184 (1975).

[30] K. Mizuno, *et al.*, *Nature* **328**, 45 (1987).

[31] A. W. Lohmann, *Particle Accelerator Utilizing Coherent Light* (1966). U.S. Patent 3267383. Filed 27th May 1963, issued 16th August 1966.

[32] A. W. Lohmann, *Particle Accelerator* (1967). Canadian Patent 773768. Issued 12th December 1967.

[33] P. S. Csonka, *Part. Accel.* **5**, 129 (1973).

[34] F. Scarlat and M. Argeşanu, *IEEE Trans. Nucl. Sci.* **24**, 1651 (1977).

[35] J. D. Lawson, *Physica Energiae Fortis et Physica Nuclearis* **5**, 339 (1981). [J. D. Lawson, *A Survey of Some Ideas for Accelerators Using Laser Light*, Tech. Rep. RL-81-030, Rutherford and Appleton Laboratories (Chilton, Oxon, UK, 1980)].

[36] B. R. Frandsen, S. A. Glasgow and J. B. Peatross, *Laser Phys.* **16**, 1311 (2006).

[37] F. Toufexis, T. Tang and S. G. Tantawi, in *Proceedings of the 36th International Free Electron Laser Conference*, (JACoW, Geneva, Switzerland, August 2014). pp. 131–136.

[38] A. M. Sessler, *IEEE Trans. Nucl. Sci.* **30**, 3145 (1983).

[39] R. B. Palmer, in *New Developments in Particle Acceleration Techniques*, ed. S. Turner, Tech. Rep. CERN-1987-011-V-2, CERN, Vol. 2 (Geneva, Switzerland, 1987). pp. 633–641. [R. B. Palmer, *Open Accelerating Structures*, Tech. Rep. SLAC-PUB-4161, Stanford Linear Accelerator Center (Stanford, CA, USA, 1986)].

[40] H. Peng and J. Zhuang, in *Proceedings of the 1979 Linear Accelerator Conference*, ed. R. L. Witkover, Tech. Rep. BNL-51134, Brookhaven National Laboratory (Upton, NY, USA, 1979). pp. 257–261.

[41] B. C. Stuart, *et al.*, *Phys. Rev. Lett.* **74**, 2248 (1995).

[42] Y. M. Oh, *et al.*, *Int. J. Heat Mass Transf.* **49**, 1493 (2006).

[43] K. Soong, *et al.*, *AIP Conf. Proc.* **1507**, 511 (2012).

[44] R. L. Byer, *AIP Conf. Proc.* **193**, 4 (1989).

[45] D. Zheng and R. L. Byer, *AIP Conf. Proc.* **335**, 156 (1995).

[46] W. Sibbett, A. A. Lagatsky and C. T. A. Brown, *Opt. Express* **20**, 6989 (2012).

[47] G. Mourou, *et al.*, *Nat. Photonics* **7**, 258 (2013).

[48] R. H. Siemann, *Phys. Rev. ST Accel. Beams* **7**, 061303 (2004).

[49] Y. C. Neil Na, R. H. Siemann and R. L. Byer, *Phys. Rev. ST Accel. Beams* **8**, 031301 (2005).

[50] M. Seidel, *et al.*, in *Proceedings of the 6th International Particle Accelerator Conference*, (JACoW, Geneva, Switzerland, 2015). pp. 2428–2433.

[51] T. Parker and P. Peck, in *Proceedings of the 55th ICFA Advanced Beam Dynamics Workshop on High Luminosity Circular e+e- Colliders*, (Geneva, Switzerland, 2014). pp. 54–58.

[52] J. Zhou, *et al.*, *Proc. SPIE* **8139**, 81390S (2011).

[53] E. A. Peralta, *et al.*, in *Proceedings of the 2011 Particle Accelerator Conference*, (PAC'11 OC / IEEE, Piscataway, NJ, USA, 2011). pp. 280–282.

[54] E. A. Peralta, *et al.*, *AIP Conf. Proc.* **1507**, 169 (2012).

[55] K. Suzuki, *Microlithography: Science and Technology*, 2nd edn. (CRC Press, Boca Raton, FL, USA, May 2007), ch. 6, pp. 329–360.

[56] A. Mizrahi and L. Schächter, *Phys. Rev. E* **70**, 016505 (2004).

[57] Z. Zhang, S. G. Tantawi and R. D. Ruth, *Phys. Rev. ST Accel. Beams* **8**, 071302 (2005).

[58] J. McNeur, *et al.*, *AIP Conf. Proc.* **1507**, 470 (2012).

[59] J. McNeur, *et al.*, in *Proceedings of the 4th International Particle Accelerator Conference*, (JACoW, Geneva, Switzerland, 2013). pp. 1307–1309.

[60] E. B. Sozer, *et al.*, in *2013 19th IEEE Pulsed Power Conference (PPC)*, (IEEE, Piscataway, NJ, USA, 2013). pp. 1–5.

[61] J. D. Lawson and M. Tigner, *Annu. Rev. Nucl. Part. Sci.* **34**, 99 (1984).

[62] G. Shvets and S. Kalmykov, *AIP Conf. Proc.* **737**, 983 (2004).

[63] S. Kalmykov, *et al.*, *AIP Conf. Proc.* **1086**, 538 (2009).

[64] B. Neuner III, *et al.*, *Phys. Rev. ST Accel. Beams* **15**, 031302 (2012).

[65] R. J. Noble, J. E. Spencer and B. T. Kuhlmey, *Phys. Rev. ST Accel. Beams* **14**, 121303 (2011).

[66] X. E. Lin, *Phys. Rev. ST Accel. Beams* **4**, 051301 (2001).

[67] R. J. Noble, *et al.*, in *Proceedings of the 2007 IEEE Particle Accelerator Conference*, (IEEE, Piscataway, NJ, USA, 2007). pp. 3103–3105.

[68] C.-K. Ng, *et al.*, *Phys. Rev. ST Accel. Beams* **13**, 121301 (2010).

[69] R. J. England, *et al.*, *IEEE J. Sel. Top. Quantum Electron.* **22**, 4401109 (2016).

[70] R. J. England, *et al.*, in *Proceedings of the 2011 Particle Accelerator Conference*, (PAC'11 OC / IEEE, Piscataway, NJ, USA, 2011). pp. 2067–2070.

[71] C. M. S. Sears, *et al.*, in *Proceedings of the 2007 IEEE Particle Accelerator Conference*, (IEEE, Piscataway, NJ, USA, June 2007). pp. 3106–3108.

[72] R. J. England, *et al.*, *AIP Conf. Proc.* **1086**, 550 (2009).

[73] B. M. Cowan, *Phys. Rev. ST Accel. Beams* **6**, 101301 (2003).

[74] B. Naranjo, *et al.*, *Phys. Rev. Lett.* **109**, 164803 (2012).

[75] B. Naranjo, *et al.*, *AIP Conf. Proc.* **1507**, 488 (2012).

[76] J. B. Rosenzweig, *et al.*, *AIP Conf. Proc.* **1507**, 493 (2012).

[77] B. Cowan, in *Proceedings of the 2005 Particle Accelerator Conference*, (IEEE, Piscataway, NJ, USA, 2005). pp. 731–733.

[78] B. M. Cowan, *Phys. Rev. ST Accel. Beams* **11**, 011301 (2008).

[79] C. McGuinness, E. Colby and R. L. Byer, *J. Mod. Opt.* **56**, 2142 (2009).

[80] C.-H. Lee, *Novel Fabrication of a 17-layer 3D Silicon-based Woodpile Structure for Dielectric Laser-Driven Accelerator*, PhD thesis, Purdue University, (West Lafayette, IN, USA, 2015).

[81] Z. Wu, *et al.*, *IEEE J. Sel. Top. Quantum Electron.* **22**, 4400909 (2016).

[82] I. Staude, *et al.*, *Opt. Express* **20**, 5607 (2012).

[83] Z. Wu, *et al.*, *Phys. Rev. ST Accel. Beams* **17**, 081301 (2014).

[84] Z. Wu, *et al.*, in *Proceedings of the 6th International Particle Accelerator Conference*, (JACoW, Geneva, Switzerland, 2015). pp. 2702–2704.

[85] J. Rosenzweig, A. Murokh and C. Pellegrini, *Phys. Rev. Lett.* **74**, 2467 (1995).

[86] R. B. Yoder and J. B. Rosenzweig, *Phys. Rev. ST Accel. Beams* **8**, 111301 (2005).

[87] R. B. Yoder and J. B. Rosenzweig, *Int. J. Mod. Phys. A* **22**, 4363 (2007).

[88] D. Bar-Lev and J. Scheuer, *Phys. Rev. ST Accel. Beams* **17**, 121302 (2014).

[89] D. Bar-Lev and J. Scheuer, in *Proceedings of CLEO: QELS-Fundamental Science*, (OSA, Washington, DC, USA, 2015). p. FW4C.8.

[90] J. Scheuer, D. Bar-Lev and A. Gover, in *High-Brightness Sources and Light-Driven Interactions*, (OSA, Washington, DC, USA, 2016). p. EM9A.4.

[91] T. Plettner, *Phase-synchronicity conditions from pulse-front tilted laser beams on one-dimensional periodic structures and proposed laser-driven deflection*, Tech. Rep. SLAC-PUB-12458, Stanford Linear Accelerator Center (Menlo Park, CA, USA, 2007).

[92] K. J. Leedle, *et al.*, *Opt. Lett.* **40**, 4344 (2015).

[93] A. Aimidula, *et al.*, in *Proceedings of the 4th International Particle Accelerator Conference*, (JACoW, Geneva, Switzerland, 2013). pp. 1283–1285.

[94] A. Aimidula, *et al.*, *Phys. Plasmas* **21**, 023110 (2014).

[95] T. Plettner, P. P. Lu and R. L. Byer, *Phys. Rev. ST Accel. Beams* **9**, 111301 (2006).

[96] E. A. Peralta, *et al.*, *Nature* **503**, 91 (2013).

[97] A. Aimidula, *et al.*, *Nucl. Instrum. Methods Phys. Res., Sect. A* **740**, 108 (2014).

[98] C.-M. Chang and O. Solgaard, *Appl. Phys. Lett.* **104**, 184102 (2014).

[99] A. Ceballos, *et al.*, in *Proceedings of the 6th International Particle Accelerator Conference*, (JACoW, Geneva, Switzerland, 2015). pp. 2717–2719.

[100] T. Plettner, R. L. Byer and P. P. Lu, in *Proceedings of the 2007 IEEE Particle Accelerator Conference*, (IEEE, Piscataway, NJ, USA, 2007). pp. 3175 – 3177.

[101] A. Szczepkowicz, *Appl. Opt.* **55**, 2634 (2016).

[102] T. Plettner and R. L. Byer, *Phys. Rev. ST Accel. Beams* **11**, 030704 (2008).

[103] T. Plettner, *et al.*, *Phys. Rev. ST Accel. Beams* **12**, 101302 (2009).

[104] T. Plettner and R. L. Byer, *Laser-Driven Deflection and Methods Involving Charged Particle Beams* (2011). U.S. Patent 7994472. Filed 16th June 2009, issued 9th August 2011.

[105] T. Plettner and R. L. Byer, *Nucl. Instrum. Methods Phys. Res., Sect. A* **593**, 63 (2008).

[106] K. P. Wootton, *et al.*, in *Proceedings of the 6th International Particle Accelerator Conference*, (JACoW, Geneva, Switzerland, 2015). pp. 2698–2701.

[107] K. Soong, *et al.*, in *Proceedings of the 2011 Particle Accelerator Conference*, (PAC'11 OC / IEEE, Piscataway, NJ, USA, 2011). pp. 292–294.

[108] K. Soong, *et al.*, *AIP Conf. Proc.* **1507**, 516 (2012).

[109] J. McNeur, *et al.*, *Elements of a dielectric laser accelerator* (2016), arXiv:1604.07684 [physics.acc-ph].

[110] J. Breuer, *et al.*, *Phys. Rev. ST Accel. Beams* **17**, 021301 (2014).

[111] J. Breuer and P. Hommelhoff, *Phys. Rev. Lett.* **111**, 134803 (2013).

[112] K. Koyama, *et al.*, *J. Phys. B: At. Mol. Opt. Phys.*

47, 234005 (2014).
[113] Y. Wei, *et al.*, *Phys. Procedia* **77**, 50 (2015).
[114] Z. Wu, *et al.*, in *Proceedings of the North American Particle Accelerator Conference 2013*, (JACoW, Geneva, Switzerland, 2013). pp. 141–143.
[115] J. Breuer, J. McNeur and P. Hommelhoff, *J. Phys. B: At. Mol. Opt. Phys.* **47**, 234004 (2014).
[116] T. Plettner, R. L. Byer and B. Montazeri, *J. Mod. Opt.* **58**, 1518 (2011).
[117] J. D. Lawson, *Contemp. Phys.* **11**, 575 (1970).
[118] K. P. Wootton, *et al.*, *Opt. Lett.* **41**, 2696 (2016).
[119] K. Koyama, *et al.*, in *Proceedings of the 3rd International Particle Accelerator Conference*, (IEEE, Piscataway, NJ, 2012). pp. 2763–2765.
[120] K. Koyama, *et al.*, *Proc. SPIE* **8779**, 877910 (2013).
[121] Y. Wei, *et al.*, in *Proceedings of the 6th International Particle Accelerator Conference*, (JACoW, Geneva, Switzerland, 2015). pp. 2618–2620.
[122] B. Montazeri Najafabadi, *et al.*, *AIP Conf. Proc.* **1507**, 476 (2012).
[123] S. Kalmykov, *et al.*, *Phil. Trans. R. Soc. A* **364**, 725 (2006).
[124] K. J. Leedle, *et al.*, *Optica* **2**, 158 (2015).
[125] J. McNeur, *et al.*, *Nucl. Instrum. Methods Phys. Res., Sect. A* **829**, 50 (2016).
[126] J. McNeur, *et al.*, *J. Phys. B: At. Mol. Opt. Phys.* **49**, 034006 (2016).
[127] R. L. Byer, *et al.*, in *Proceedings of the 1999 Particle Accelerator Conference*, (IEEE, Piscataway, NJ, 1999). pp. 321–324.
[128] R. Noble, *et al.*, in *Proceedings of the 2003 Particle Accelerator Conference*, (IEEE, Piscataway, NJ, USA, 2003). pp. 1858–1860.
[129] E. Colby, *et al.*, in *Proceedings of the Particle Accelerator Conference 2005*, (IEEE, Piscataway, NJ, USA, May 2005). pp. 2024–2026.
[130] E. Colby, *et al.*, in *Proceedings of the Particle Accelerator Conference 2007*, (IEEE, Piscataway, NJ, USA, June 2007). pp. 3115–3117.
[131] P. Musumeci, J. Moody and G. Gatti, in *Proceedings of the Particle Accelerator Conference 2007*, (IEEE, Piscataway, NJ, 2007). pp. 2751–2753.
[132] S. Otsuki, *et al.*, in *Proceedings of the 5th International Particle Accelerator Conference*, (JACoW, Geneva, Switzerland, 2014). pp. 1434–1436.
[133] M. Uesaka, *et al.*, *IOP Conf. Ser.: Mater. Sci. Eng.* **79**, 012015 (2015).
[134] K. Koyama, *et al.*, in *Proceedings of the 7th International Particle Accelerator Conference*, (JACoW, Geneva, Switzerland, May 2016). pp. 1585–1587.
[135] H. Okamoto, *et al.*, in *Proceedings of the 7th International Particle Accelerator Conference*, (JACoW, Geneva, Switzerland, May 2016). pp. 4070–4072.
[136] P. A. McIntosh, *et al.*, in *Proceedings of the 4th International Particle Accelerator Conference*, (JACoW, Geneva, Switzerland, 2013). pp. 3708–3710.
[137] Y. Wei, *et al.*, in *Proceedings of the 7th International Particle Accelerator Conference*, (JACoW, Geneva, Switzerland, 2016). pp. 1970–1972.
[138] U. Dorda, *et al.*, *Nucl. Instrum. Methods Phys. Res., Sect. A* **829**, 233 (2016).
[139] J. Zhu, *et al.*, *Phys. Rev. Accel. Beams* **19**, 054401 (2016).
[140] J. Zhu, *et al.*, in *Proceedings of the 7th International Particle Accelerator Conference*, (JACoW, Geneva, Switzerland, 2016). pp. 3244–3246.
[141] E. A. Peralta, *Accelerator on a Chip: Design, Fabrication, and Demonstration of Grating-based Dielectric Microstructures for Laser-driven Acceleration of Electrons*, PhD thesis, Stanford University, (2015).
[142] K. Soong, *Particle accelerator on a wafer: demonstration of electron acceleration and diagnostics with microstructures*, PhD thesis, Stanford University, (2014).
[143] R. J. England, *et al.*, in *Proceedings of the 3rd International Particle Accelerator Conference*, (IEEE, Piscataway, NJ, USA, 2012). pp. 1050–1053.
[144] X. H. Lu, *et al.*, *Phys. Rev. ST Accel. Beams* **18**, 032802 (2015).
[145] P. Hommelhoff, *et al.*, *Ultramicrosc.* **109**, 423 (2009).
[146] T. Juffmann, *et al.*, *Phys. Rev. Lett.* **115**, 264803 (2015).
[147] F. Süßmann, M. F. Kling and P. Hommelhoff, *From Attosecond Control of Electrons at Nano-Objects to Laser-Driven Electron Accelerators*, in *Attosecond Nanophysics*, eds. P. Hommelhoff and M. F. Kling (Wiley-VCH Verlag GmbH & Co. KGaA, Weinheim, Germany, 2015), ch. 6, pp. 155–196.
[148] G. Travish, *et al.*, in *Proceedings of the 3rd International Particle Accelerator Conference*, (IEEE, Piscataway, NJ, USA, May 2012). pp. 2738–2740.
[149] R. B. Yoder, *et al.*, in *Proceedings of the 6th International Particle Accelerator Conference*, (JACoW, Geneva, Switzerland, 2015). pp. 2624–2626.
[150] M. Kozák, *et al.*, *Optical gating and streaking of free-electrons with attosecond precision* (2015), arXiv:1512.04394 [physics.optics].
[151] P. Bermel, *et al.*, *Nucl. Instrum. Methods Phys. Res., Sect. A* **734, Part A**, 51 (2014).
[152] K. R. Hogstrom and P. R. Almond, *Phys. Med. Biol.* **51**, R455 (2006).
[153] J. E. Clayton and P. A. Lovoi, *Laser Accelerator Driven Particle Brachytherapy Devices, Systems and Methods* (2015). U.S. Patent 9022914 B2. Filed 30th September 2011, issued 5th May 2015.
[154] H. O. Wyckoff, *et al.*, *Radiation Dosimetry: Electron Beams with Energies Between 1 and 50 MeV*, Tech. Rep. 35, International Commission on Radiation Units and Measurements (Bethesda, MD, USA, 1984).

[155] M. Abe and M. Takahashi, *Int. J. Radiat. Oncol. Biol. Phys.* **7**, 863 (1981).
[156] J. R. Palta, *et al.*, *Int. J. Radiat. Oncol. Biol. Phys.* **33**, 725 (1995).
[157] C. G. Willett, B. G. Czito and D. S. Tyler, *J. Clin. Oncol.* **25**, 971 (2007).
[158] J. S. Vaidya, *et al.*, *Lancet* **376**, 91 (2010).
[159] M. Totzeck, *et al.*, *Nat. Photonics* **1**, 629 (2007).
[160] G. E. Moore, *Electron.* **38**, 114 (1965).
[161] Z. T. Zhao, *Rev. Accel. Sci. Technol.* **03**, 57 (2010).
[162] M. E. Couprie, *J. Electron Spectrosc. Relat. Phenom.* **196**, 3 (2014).
[163] P. Naulleau, in *Proceedings of the 6th International Particle Accelerator Conference*, (JACoW, Geneva, Switzerland, 2015). p. MOYGB1.
[164] B. E. Carlsten, *et al.*, *Nucl. Instrum. Methods Phys. Res., Sect. A* **622**, 657 (2010).
[165] W. A. Barletta, *et al.*, *Nucl. Instrum. Methods Phys. Res., Sect. A* **618**, 69 (2010).
[166] P. S. Csonka, *Part. Accel.* **7**, 9 (1975).
[167] Y.-C. Huang, *et al.*, *Phys. Rev. ST Accel. Beams* **18**, 080701 (2015).
[168] T. Plettner, *DC high-voltage super-radiant free-electron based EUV source* (2015). U.S. Patent 9053833 B2. Filed 27th February 2013, issued 9th June 2015.
[169] R. J. England, *et al.*, in *Proceedings of the 2013 North American Particle Accelerator Conference*, (JACoW, Geneva, Switzerland, 2013). pp. 129–131.
[170] R. J. England, in *High-Brightness Sources and Light-Driven Interactions*, (OSA, Washington, DC, USA, 2016). p. ET3A.2.
[171] K. Soong and R. L. Byer, *Opt. Lett.* **37**, 975 (2012).
[172] K. Soong, *et al.*, in *Proceedings of the 2013 North American Particle Accelerator Conference*, (JACoW, Geneva, Switzerland, 2013). pp. 138–140.
[173] K. Soong, *et al.*, *Opt. Lett.* **39**, 4747 (2014).
[174] J.-K. So, *et al.*, *ACS Photonics* **2**, 1236 (2015).
[175] M. Kozák, *et al.*, *Opt. Lett.* **41**, 3435 (2016).

K. P. Wootton earned the BSc(Hons) and BE(Hons) degrees from Monash University in 2010, and the PhD degree in physics from the University of Melbourne in 2014. Presently, he is an Experimental Research Associate at SLAC National Accelerator Laboratory. His research interests include dielectric laser accelerators, ultralow vertical emittance electron beams, spin-polarized beams, and beam diagnostics based on synchrotron light and undulator radiation. Dr. Wootton is a member of the Australian Institute of Physics and the American Physical Society.

J. McNeur earned a BSc in Physics and a BSc in Mathematics from the University of Chicago in 2007. He earned his PhD from The University of California – Los Angeles in 2014. He is currently a Postdoctoral Scholar in the Laser Physics Department at the Friedrich-Alexander-Universität Erlangen-Nürnberg, with research interests including novel high gradient acceleration techniques, ultrafast electron sources, nanophotonics, and attosecond physics.

K. J. Leedle earned the BS in Electrical Engineering from the University of Wisconsin–Madison in 2010. He was awarded the PhD degree in Electrical Engineering from Stanford University in 2016. He is currently a Postdoctoral Scholar in the Department of Electrical Engineering at Stanford University. His research interests include dielectric laser accelerators, ultrafast optics, electron optics, and nanophotonics. Dr. Leedle is a member of The Optical Society.